Heat stress destabilizes symbiotic nutrient cycling in corals

Nils Rädecker[1,2,3*], Claudia Pogoreutz[1,3], Hagen M. Gegner[1,4], Anny Cardenas[1,3], Florian Roth[1,5,6], Jeremy Bougoure[7], Paul Guagliardo[7], Christian Wild[8], Mathieu Pernice[9], Jean-Baptiste Raina[9], Anders Meibom[2,10], Christian R. Voolstra[1,3]

[1] Red Sea Research Center, Division of Biological and Environmental Science and Engineering, King Abdullah University of Science and Technology, Thuwal, Saudi Arabia

[2] Laboratory for Biological Geochemistry, School of Architecture, Civil and Environmental Engineering, École Polytechnique Fédérale de Lausanne, Lausanne, Switzerland

[3] Department of Biology, University of Konstanz, Konstanz, Germany

[4] Metabolomics Core Technology Platform, Centre for Organismal Studies, University of Heidelberg, Heidelberg, Germany

[5] Baltic Sea Centre, Stockholm University, Stockholm, Sweden

[6] Faculty of Biological and Environmental Sciences, Tvärminne Zoological Station, University of Helsinki, Helsinki, Finland

[7] Centre for Microscopy, Characterisation and Analysis, University of Western Australia, Perth, WA, Australia

[8] Marine Ecology Department, Faculty of Biology and Chemistry, University of Bremen, Bremen, Germany

[9] Climate Change Cluster, University of Technology Sydney, Sydney, Australia

[10] Center for Advanced Surface Analysis, Institute of Earth Sciences, Université de Lausanne, Lausanne, Switzerland

* to whom correspondence should be addressed: nils.radecker@kaust.edu.sa

ORCID iDs

Nils Rädecker	Claudia Pogoreutz	Hagen M. Gegner	Anny Cardenas
0000-0002-2387-8567	0000-0002-2853-7673	0000-0001-7374-7197	0000-0002-4080-9010
Florian Roth	Jeremy Bougoure	Paul Guagliardo	Christian Wild
0000-0003-4004-5863	0000-0002-4869-035X	0000-0003-3488-6754	0000-0001-9637-6536
Mathieu Pernice	Jean-Baptiste Raina	Anders Meibom	Christian R. Voolstra
0000-0002-3431-2104	0000-0002-7508-0004	0000-0002-4542-2819	0000-0003-4555-3795

Classification

Biological Sciences -> Ecology

Keywords

coral bleaching, endosymbiosis, metabolic interaction, resource competition, selfish symbiont

Author contributions

N.R., C.P., M.P., JB.R., and CR.V. conceived the experiment. N.R., C.P., H.G., F.R. conducted the experiment. N.R., A.C., J.B., P.G., performed sample and data analysis. All authors contributed to writing and revising the manuscript.

Abstract

Recurrent mass bleaching events are pushing coral reefs worldwide to the brink of ecological collapse. While the symptoms and consequences of this breakdown of the coral–algal symbiosis have been extensively characterized, our understanding of the underlying causes remains incomplete. Here, we investigated the nutrient fluxes and the physiological as well as molecular responses of the widespread coral *Stylophora pistillata* to heat stress prior to the onset of bleaching to identify processes involved in the breakdown of the coral–algal symbiosis. We show that altered nutrient cycling during heat stress is a primary driver of the functional breakdown of the symbiosis. Heat stress increased the metabolic energy demand of the host, which was compensated by the catabolic degradation of amino acids. The resulting shift from net uptake to release of ammonium subsequently promoted the growth of algal symbionts and retention of photosynthates. Together, these processes form a feedback loop that gradually leads to the decoupling of carbon translocation from the symbiont to the host. Energy limitation and altered symbiotic nutrient cycling are, thus, key factors in the early heat stress response, directly contributing to the breakdown of the coral–algal symbiosis. Interpreting the stability of the coral holobiont in light of its metabolic interactions provides a missing link in our understanding of the environmental drivers of bleaching and may ultimately help uncover fundamental processes underpinning the functioning of endosymbioses in general.

Significance Statement

Ocean warming is causing repeated mass coral bleaching, leading to catastrophic losses of coral reefs worldwide. Our ability to slow or revert this decline is hampered by an incomplete understanding of the processes underlying the breakdown of the coral–algal symbiosis. Here, we show that heat stress destabilizes the nutrient cycling between corals and their endosymbiotic algae long before bleaching becomes apparent. Notably, increased metabolic energy demands shift the coral–algal symbiosis from a nitrogen- to a carbon-limited state reducing translocation and recycling of photosynthetic carbon. This effectively undermines the ecological advantage of harboring algal symbionts and directly contributes to the breakdown of the coral-algal symbiosis during heat stress.

Main Text

Introduction

Coral reef ecosystems are suffering a dramatic decline worldwide due to the effects of anthropogenic environmental change (1, 2). The steadily increasing rate of ocean warming is now the main driver of reef degradation due to recurrent mass bleaching of corals (3); i.e., the expulsion or digestion of endosymbiotic algae by their coral host during extended periods of heat stress. Given that the rate of global warming appears to exceed the adaptive capacity of many corals, novel approaches are required to mitigate the effects of climate change on coral reefs (4). Importantly, the bleaching susceptibility of the coral holobiont, i.e. the functional ecological unit composed of the coral host and its associated microbes (5), does not depend on temperature stress alone (6, 7). Rather, the response of the coral holobiont during heat stress is determined by the interactions between all holobiont members and must be understood in the context of their given environment (8). Consequently, differences in host identity, microbiome community composition, as well as abiotic and biotic environmental conditions result in differential bleaching susceptibility from organismal to ecosystem scales (9, 10). This heterogeneity in bleaching susceptibility could be harnessed for active conservation measures to preserve the functioning of reefs in the future (11). Our ability to predict or mitigate the consequences of climate change on coral reefs, thus, requires an in-depth understanding of the processes underlying the breakdown of the coral–algal symbiosis during heat stress.

Molecular and ultrastructural evidence suggests that the loss of algal symbiont cells during bleaching in its essence is the result of an innate immune response of the coral host (12). Prevailing theories suggest that this immune response is initially triggered by the excess production and release of reactive oxygen species (ROS) by the algal symbionts due to photoinhibition (13). Indeed, heat stress does promote an increased ROS release by algal symbionts and the quenching of ROS via the addition of antioxidants has been shown to attenuate the severity of bleaching in corals (14, 15). Yet, recent observations have challenged the notion of photosynthetic ROS production as the only direct driver of coral bleaching: I. Bleaching also occurs in the dark without photosynthetic ROS production (16). II. Oxidative stress in the host tissue during heat stress may precede the photoinhibition of algal symbionts (17). III. Extracellular levels of superoxide do not correlate with symbiont abundance or bleaching status of corals during heat stress (18). Taken together, these studies suggest that the role of symbiotic ROS production in triggering coral bleaching is more complex than previously thought, and that additional cellular processes may be involved.

Efficient assimilation and recycling of organic and inorganic nutrients provide the functional basis of the coral–algal symbiosis and is the key to the ecological success of corals in highly oligotrophic waters (19). Photosynthates derived from the algal metabolism constitute the main energy source for the coral host (20). The ability of corals to cope with environmental stress, therefore, depends on carbon translocation by algal symbionts (21). In a stable state, nitrogen limitation of algal symbionts causes the accumulation and subsequent release of excess photosynthetic carbon to the coral host, thereby ensuring the functioning of the symbiosis (22–24). Therefore, the stability of the symbiosis during stress may ultimately depend on environmental nitrogen availability and the ability of the host to control algal nitrogen uptake under these conditions (25, 26). Indeed, it is now apparent that the nutritional status and environmental nutrient availability can affect the bleaching susceptibility of corals during heat stress (27–30). Likewise, elevated temperatures at sub-bleaching levels have been

linked to alterations in nitrogen uptake and carbon translocation in the coral–algal symbiosis (31, 32). Taken together, these studies suggest that symbiotic nutrient exchange may play a critical role in the onset of coral bleaching (26). However, the underlying causes of altered nutrient cycling between coral and algae, the nature of these metabolic interactions, and their consequences for the functioning of the symbiosis are poorly understood.

Here, we investigated the effect of heat stress on metabolic interactions in the coral–algal symbiosis and their consequences for holobiont functioning in a three-week-long heat stress experiment. To identify the primary processes initiating the destabilization of the symbiosis, we focused on early stress responses prior to any visual signs of bleaching, combining physiological and molecular approaches (host and symbiont gene expression) with quantification of nutrient fluxes (carbon and nitrogen) at the holobiont and cellular level.

Results & Discussion

Coral bleaching takes time

The Red Sea system is home to some of the most thermotolerant corals on the planet and has been identified as a potential refuge for corals during climate change (33–35). We exposed colonies of *Stylophora pistillata* from the central Red Sea to conditions reflecting the annual mean (29.1 °C; control) or summer maximum (32.9 °C; heat stress with 3 days of gradual temperature acclimation) temperature for the collection site in 2017 (Fig. S1). After 21 days of heat stress, *S. pistillata* colonies showed clear signs of bleaching as reflected in a visual loss of pigmentation, corresponding to 78 % and 67 % decline in algal symbiont densities and chlorophyll *a* content, respectively (Fig. S2, see Tab. S1 for statistical results). This observation confirms that corals from the central Rea Sea live close to their upper temperature tolerance limits and is consistent with the notion that the cumulative heat stress history, rather than acute temperature stress, determines the bleaching threshold of a coral colony (36).

Oxidative damage in the coral host prior to coral bleaching

To understand the underlying processes that cause the breakdown of the coral–algal symbiosis during prolonged heat stress, we investigated the physiological performance and metabolic interactions of symbiotic partners on day 10 of the experiment, i.e., after 7 days at maximum temperature, but before visible bleaching commenced (Fig. S1E). At this time point, *S. pistillata* colonies did not exhibit any visual change in pigmentation or decreases in symbiont density and chlorophyll *a* content between heat stress and control temperatures (Fig. 1A-C). Despite the apparent integrity of the symbiosis at this time point, heat stress had pronounced effects on coral–algal interactions. Although maximum photosynthetic efficiency only exhibited a small reduction (7 %) (Fig. S3A), the relative ROS leakage from freshly isolated symbionts increased by 45 % under heat stress. This correlated with a significant increase in the level of oxidative damage in the coral host, as reflected in increased levels of lipid peroxidation (Fig. 1D). Such oxidative damage in response to symbiotic ROS production is often considered to be the direct cellular trigger for symbiont loss during coral bleaching. Yet, in the present study, increased oxidative damage preceded the onset of visual bleaching by 10 days (bleaching was first visually discernible on day 20 of the experiment). Consequently, coral bleaching does not appear to be directly and causally connected to the increased symbiotic ROS production per se. If oxidative

stress was indeed the main trigger of subsequent bleaching, the resulting oxidative damage must have gradually accumulated and/or the ability of the coral holobiont to cope with oxidative stress was gradually reduced – and eventually overwhelmed – over the course of the experiment.

Dual RNA-Seq identifies primary heat stress responses in the coral–algal symbiosis

To further elucidate the early stress response, we investigated the transcriptomic response of host and symbionts to heat stress on day 10 of the experiment, i.e. prior to the onset of bleaching (Fig. S1E). At this time-point, overall gene expression profiles of the coral host and algal symbionts were largely determined by the different mother colonies, accounting for 79 % and 66 % of the total variation, respectively (Fig. S4A,B, Tab. S2, Tab. S3). In contrast, heat stress only explained 12 % and 17 % of the variation in coral host and algal symbiont gene expression, reflecting the apparent integrity of the symbiosis at this time point. However, subsets of genes related to individual EuKaryotic Orthologous Groups (KOGs) showed a pronounced stress response. In particular, genes related to 'energy production and conversion' showed strong differential expression due to heat stress in coral hosts and algal symbionts alike (Fig. S4C,D). This observation aligns with the predictions of the Metabolic Theory of Ecology, which holds that increased metabolic turnover is a direct consequence of elevated temperatures in the coral holobiont (37). Consistently, the observed changes in gene expression indicated that altered energy metabolism is part of the earliest response to heat stress in the coral–algal symbiosis.

Heat stress induces coral host starvation and amino acid degradation

On day 10, a total of 3,426 genes, out of the 25,769 present in *S. pistillata (38)*, were significantly differentially expressed (1,699 up- and 1,727 downregulated) (Suppl. Data). Gene set enrichment analysis revealed 273 significantly enriched biological processes (Suppl. Data). In addition to genes involved in well-characterized heat stress responses (stress sensing, protein folding, DNA replication & repair, and immune responses), genes linked to energy and amino acid metabolism were among the most differentially expressed (Fig. S4E). Notably, heat stress prompted the downregulation of genes related to transport and metabolism of cellular energy substrates, such as lipids, fatty acids, and sugars. Genes associated with key processes in the cellular energy supply, such as the tricarboxylic acid (TCA) cycle and adenosine triphosphate (ATP) synthesis and metabolism, were also consistently downregulated (Fig. 2D, Fig. S4E). Taken together, the observed expression patterns point to a state of energy starvation in the coral host as a result of carbon limitation during heat stress.

As a likely consequence of this energy limitation, patterns of altered amino acid cycling reflected an increased use of amino acids as alternative energy substrates during heat stress. Catabolic degradation pathways for several amino acids showed a strong upregulation while key amino acid biosynthesis pathways were downregulated (Fig. S4E). In particular, glutamate metabolism, which plays a key role in the connection between anabolic and catabolic processes (39), exhibited strong differential regulation. Glutamate can be synthesized from α-ketoglutarate generated in the TCA cycle via the fixation of ammonium (NH_4^+). In a stable symbiosis, glutamate synthesis enables the coral host to utilize photosynthetically fixed and translocated carbon for amino acid and protein synthesis (23). Yet we observed that, as a result of heat stress, the expression of two key host genes in the biosynthesis of glutamate, glutamine synthetase (GS) and glutamate synthase (GOGAT), were downregulated (Fig.

2A-D). At the same time, genes encoding glutamate dehydrogenase (GDH) showed either an upregulation (2 genes) or a downregulation (1 gene). GDHs facilitate the anabolic synthesis of glutamate as well as the catabolic degradation of glutamate to fuel the TCA cycle. Interestingly, in contrast to most animals, corals possess distinct isoenzymes of GDH for the anabolic and catabolic reactions, respectively (40). The observed changes in expression of GDH genes may thus reflect opposing regulations of anabolic and catabolic reactions; i.e., the downregulation of anabolic and upregulation of catabolic enzymes. Importantly, the pattern of GDH gene regulation observed in *S. pistillata* during heat stress was opposite to that observed in symbiotic (nitrogen-limited) compared to aposymbiotic (carbon-limited) Aiptasia (*Exaiptasia pallida*) sea-anemones (23) suggesting downregulation of anabolic glutamate synthesis and upregulation of catabolic glutamate degradation. These alterations of the coral host glutamate metabolism and amino acid cycling observed on day 10 can thus be a direct consequence of energy limitation of the coral host's metabolism due to heat stress. Such a starvation-driven shift from synthesis to degradation of amino acids is expected to result in greater production of NH_4^+ and reduced assimilation of environmental nitrogen by the coral host during heat stress (Fig. 2D). Consequently, starvation of the coral host may directly lead to increased nitrogen availability within the holobiont during heat stress.

Increased ammonium availability alleviates nitrogen limitation of algal symbionts

The transcriptomic response of algal symbionts was closely linked to the response of the coral host. Out of the 49,109 genes of *Symbiodinium microadriaticum* (41), 1,979 genes showed significant differential expression (861 up- and 1,118 downregulated) on day 10 (Suppl. Data). Gene set enrichment analysis revealed 82 significantly enriched biological processes (Suppl. Data). In particular, nitrogen assimilation pathways were among the most affected processes in the algal symbiont (Fig. S4F). In contrast to the coral host, algal symbionts possess the cellular machinery for assimilatory nitrate (NO_3^-) reduction (42). Yet, during heat stress, expression of genes encoding high-affinity nitrate transporters (NRT), nitrate reductases (NR), and nitrite reductases (NIR) showed consistent downregulation (Fig. 2E-G). In combination with the downregulation of several NH_4^+ transporters, this indicated that algal symbionts invested fewer resources into the uptake of nitrogen from their environment. However, glutamate synthesis via the GS-GOGAT pathway showed no significant downregulation, suggesting that active NH_4^+ fixation was maintained. Consequently, the observed alterations in algal nitrogen assimilation pathways point to increased NH_4^+ availability in the holobiont consistent with the heat stress-induced perturbation of the host nitrogen cycle discussed above (Fig. 2D).

Nitrogen limitation is critical to control the algal symbiont population in the coral holobiont (25). Without nitrogen limitation, the algal symbionts will begin to proliferate and consume photosynthetically-fixed carbon until no excess carbon is available for translocation to the host (22–24). Downregulation of carbohydrate catabolism and ATP metabolism may reflect the reduced availability of excess carbon in algal symbiont cells (Fig. S4F). In contrast to the coral host, however, heat stress did not cause a consistent downregulation of the TCA cycle in algal symbionts (Fig. S4F), suggesting that photosynthetic carbon availability was still sufficient to fulfill their energy demands and growth. In summary, algal symbiont gene expression during heat stress consistently pointed to increased nitrogen availability that stimulated the growth of algal symbionts and reduced availability of photosynthetic carbon for translocation to the host.

Retention of photosynthates by algal symbionts further reduces carbon availability for the coral host

The altered expression of genes associated with key symbiotic nutrient cycling pathways on day 10 was corroborated by drastic changes in the uptake and cycling of nutrients in the symbiosis. The respiration rate increased by 46% at the holobiont level reflecting an increased metabolic turnover and higher energy demand during heat stress (Fig. 3A). The increase in respiratory carbon consumption was only partially compensated by a 27 % stimulation of gross photosynthesis rates, likely due to increased CO_2 availability (43). In light of the changes in coral host gene expression outlined above, this net increase in respiratory carbon consumption was not sufficiently compensated by heterotrophic feeding resulting in the consumption of energy reserves. This overall reduction in organic carbon availability also caused a 66 % drop in the release of dissolved organic carbon (DOC) from the holobiont (Fig. S3B).

Nanoscale secondary ion mass spectrometry (NanoSIMS) quantitative imaging of $H^{13}CO_3$ assimilation and photosynthate translocation revealed that these alterations in carbon availability were not evenly distributed between symbiotic partners. A 24 h incubation with $H^{13}CO_3$ on day 10 (see M&M for details) showed that while the ^{13}C enrichment of symbiont cells increased by 36 % (relative to control conditions), the ^{13}C enrichment of the surrounding host tissue decreased by 26 % (Fig. 3B-D). These ^{13}C enrichment levels reflect the anabolic incorporation of labeled photosynthetic carbon as well as its catabolic consumption in the respective tissue. The contrasting responses in ^{13}C enrichment levels of the coral host and algal symbiont during heat stress thus reflect the combined result of higher metabolic carbon turnover in the host tissue and a reduced translocation of photosynthetic carbon by the algal symbionts. Consequently, the reduced availability of phototrophic carbon at the holobiont level was detrimental to the coral host, but not to the algal symbionts.

Increased nitrogen availability promotes growth of algal symbionts

Changes in algal gene expression on day 10 suggest that the observed retention of photosynthates by algal symbionts is the direct consequence of increased nitrogen availability during heat stress. Indeed, heat stress resulted in a shift from a net uptake to a strong net release of NH_4^+ at the holobiont level at this time point, likely reflecting the increased production of NH_4^+ by the coral host's amino acid catabolism (Fig. 3E). This excess NH_4^+ availability was directly reflected in the assimilation of NH_4^+ from the surrounding seawater by both symbiotic partners. NanoSIMS imaging revealed 53 % and 36 % reduction in $^{15}NH_4^+$ assimilation in algal symbionts and surrounding coral host tissue, respectively, during a 24 h labeling incubation on day 10 (see M&M for details) (Fig. 3F-H). This is consistent with an increase in the recycling of intrinsically generated unlabeled NH_4^+. In line with this, the reduced dependency on environmental nitrogen sources was further confirmed by a 61 % decline in net nitrate (NO_3^-) uptake rates at the holobiont level during heat stress (Fig. 3I). NanoSIMS quantification of $^{15}NO_3^-$ assimilation during a 24 h incubation on day 10 revealed an 81 % and 88 % decline in ^{15}N enrichment levels of algal symbionts and coral host tissue, respectively.

To assess the net effect of altered nitrogen cycling on algal symbionts, we estimated the proportion of dividing cells in hospite from NanoSIMS images (Fig. 4A,B). The mitotic index of algal symbiont populations showed an approximately three-fold increase during heat stress (Fig. 4C). This increase in

algal proliferation during heat stress is consistent with an enhanced nitrogen availability for the algal symbionts and explains the increased retention of photosynthates for their growth.

Dynamic nutritional states in the coral–algal symbiosis

The observed alterations in nutrient cycling in the present study paint a clear picture of the metabolic state of the coral–algal symbiosis prior to the onset of bleaching (day 10 of heat stress). At the same time, our results allow the identification of feedback loops that directly affect the stability of the coral–algae symbiosis over time: I. Heat stress reduces energy availability for the host. II. The resulting shift in amino acid metabolism increases nitrogen availability for the algal symbionts, which begin to grow and divide faster. III. This, in turn, reduces carbon translocation to the coral host, setting up a positive feedback loop that exacerbates host energy starvation.

While elevated temperatures may initially only mildly affect energy availability in the coral host, the positive feedback of these processes will gradually lead to more pronounced alterations in the nutrient cycling status between host and symbiont during prolonged heat stress. Over time, these processes eventually lead to a collapse of carbon translocation by the symbiont, which undermines the ecological advantage of this symbiosis for the host (Fig. 5). Elevated temperatures, however, do not necessarily force corals on a one-way road to bleaching. The positive feedback loop outlined above can be compensated for by negative feedback loops. Our experiment identified one such potential mechanism that may stabilize symbiotic nutrient cycling during elevated temperatures. Specifically, we observed that increased nitrogen availability stimulated algal cell division rates during heat stress. The proliferation of algal symbionts directly translates into increased nitrogen demand as more biomass has to be sustained. If the rate of increase in nitrogen availability does not exceed the increase in nitrogen demand due to algal symbiont growth, carbon translocation to the host may be sustained or even increased during elevated temperatures, as more algal cells perform photosynthesis. This hypothesis is consistent with observations showing that corals hosting a fast-growing symbiont were more resistant to heat stress-induced bleaching than corals hosting a slow-growing symbiont type (44).

Taken together, our findings suggest that the state of nutrient cycling is dependent on the dynamic equilibrium between positive and negative feedback loops outlined above (Fig. 5). In a stable state, the coral host and algal symbionts compete for available nitrogen. Moderate rates of warming increase metabolic energy demand, yet these effects may be balanced by stimulated symbiont growth. In contrast, rapid warming likely alters symbiotic nutrient cycling at a rate that cannot be compensated for by symbiont proliferation. Under such conditions carbon translocation by the symbionts will gradually decrease, ultimately shifting both symbiotic partners towards a carbon-limited state. Interestingly, the same processes that destabilize nutrient exchange during heat stress may, in reverse order, lead to the onset of nutrient exchange during the (re-)infection of the coral host with symbionts. Symbiont-free corals are in a carbon-limited state (23, 45). As such, initial colonizing symbionts can rapidly proliferate due to high nitrogen availability. As symbiont densities increase, algae start competing with each other for available nitrogen (22). Being nitrogen-limited in their growth, symbionts will start releasing excess organic carbon to the host, thereby gradually shifting the system to a nitrogen-limited state characteristic of a stable symbiosis (Fig. 5).

What triggers coral bleaching?

The loss of algal symbionts is not the direct cause of coral mortality during bleaching (46). Rather, mortality is caused by the starvation of the coral host that follows a decrease in phototrophic carbon input by the algae (46). Here, we have shown that heat stress destabilizes symbiotic carbon translocation before the actual expulsion of the algal symbiont, i.e., prior to any visible signs of bleaching. Consequently, corals can experience severe energy starvation even before algal symbiont abundance is reduced. As such, the loss of symbionts itself may not be of (direct) negative consequence for the coral host, since it may allow association with faster-growing symbionts that can sustain carbon translocation even under elevated temperatures (44, 47).

At this point, the cellular trigger of algal symbiont expulsion remains unknown. Previous studies proposed that ROS levels and oxidative damage in the coral host tissue may be an important cue for coral bleaching (48). The level of oxidative damage depends on the interplay of ROS production, antioxidant capacity, and cellular repair processes (12). Therefore, alterations in cellular energy availability, as observed here, will directly affect the ability of the host to cope with oxidative stress and thereby determine the temperature threshold of bleaching in corals. In addition, Hill & Hill (49) proposed that the arrest of maturation of the phagosome surrounding the symbiont depends on its release of photosynthates to mimic the digestion of prey. In this light, altered symbiotic nutrient cycling, i.e. the cessation of photosynthate transfer, may be the ultimate cause of symbiont expulsion. Our findings suggest that heat stress gradually reduces carbon translocation by the symbionts, ultimately shifting the symbiotic system to a carbon-limited state. Eventually, carbon release by the algal symbiont may be insufficient to maintain phagosome arrest. As the phagosome matures, the symbiont would either be digested or expelled from the coral host cell (50), thereby causing coral bleaching. Hence, the stability of the coral holobiont during heat stress directly depends on the state of nutrient cycling in the coral–algal symbiosis.

Conclusion

Our efforts to preserve coral reefs in the Anthropocene are hampered by an incomplete understanding of the processes underpinning susceptibility and resilience of corals to heat stress. Our study demonstrates that heat stress destabilizes symbiotic nutrient cycling well before the actual breakdown of the coral–algal symbiosis. Therefore, thermal history rather than thermal bleaching thresholds may provide a better proxy to predict the resilience of corals to heat stress. Future research efforts should consider bioenergetics and the nutritional status of host and symbiont in the context of environmental conditions. As such, the performance of algal symbionts during heat stress should be assessed based on their nutrient cycling properties and growth rates, rather than ROS production alone. Considering the effects of the local biotic and abiotic environment on the mechanisms underlying symbiotic nutrient cycling identified in this study will improve our ability to predict coral thermotolerance and help identify regions of particular interest for conservation management to mitigate the effects of climate change.

Material and Methods

Sampling site, coral collection, and experimental design

Corals were collected from Abu Shoosha reef near the Saudi Arabian central Red Sea coast (Fig. S1). Temperatures were monitored at a water depth of ~5m throughout the year 2017 with HOBO pendant temperature loggers (Onset, US) to identify annual mean (29.1 °C) and maximum temperatures (32.9 °C) representative for a non-bleaching year in the region. In summer 2018, five colonies of *S. pistillata* (⌀ > 30 cm) were collected at the same location and depth and immediately transported to the aquaria facility at the Coastal and Marine Resources core lab at King Abdullah University of Science and Technology. Colonies were fragmented into 20 nubbins each, which were distributed over two 150 L aquaria per colony (total of 10 aquaria; one tank assigned for each treatment in the experiment). All tanks were filled with freshly collected seawater from Abu Shoosha reef (salinity = 40.1; NH_4^+ = 0.48 µM; NO_3^- = 0.19 µM; PO_4^{3-} = 0.03 µM) with a daily water renewal rate of 25 % and maintained at a light regime resembling *in situ* conditions (peak daytime irradiation = 750 µmol quanta m^{-2} s^{-1}) and constant temperature of 29.1 ˚C.

After seven days of acclimation, the five aquaria assigned to the heat stress treatment were gradually ramped to a temperature of 32.9 °C (maximum temperature of 2017) over the course of three days while the remaining five aquaria were maintained at a temperature of 29.1 °C (mean temperature of 2017) as control conditions (Figure S1). Corals were sampled after 10 days (i.e., 7 days at maximum temperature) and after 21 days (when visual bleaching was observed). On day 10, a range of response parameters was assessed to identify primary physiological, molecular, and metabolic responses of the coral–algal symbiosis to heat stress (see below for details). In contrast, on day 21 only symbiont density and chlorophyll *a* content was recorded to quantify the extent of bleaching. For all response parameters, one sample per colony and treatment was collected (i.e., n = 5 for each condition). All incubation measurements were performed on the day of sampling. For all other measurements, fragments were snap-frozen in liquid N_2 and stored at -80 °C for later processing.

Algal symbiont density and chlorophyll a *content*

Frozen coral fragments were placed into individual Ziploc bags and doused in 7.5 mL of ice-cold PBS buffer (1x). All tissue was removed from the coral skeleton using air pressure and the resulting tissue slurry was transferred into a falcon tube and homogenized for 30 s with a T-18 UltraTurrax (IKA, Germany) on ice. Symbiont cells were washed in three cycles of centrifugation (3,000 g) and resuspension in PBS. For symbiont density, three technical replicates of 200 µL were transferred into a 96-well plate through a cell strainer (40 µm mesh size). Symbiont concentrations were quantified by flow cytometry using the BD LSRFortessa (BD Biosciences, US) with an excitation wavelength of 488 nm and fluorescence emission detection at 695/40 nm. Subsequent gating of recorded events was done in FlowJo v.10.5.3 based on forward scatter and chlorophyll autofluorescence. For chlorophyll content analysis, 1 mL of washed symbiont cell suspension was transferred into an Eppendorf Tube, pelleted, and resuspended in acetone (100 %). Samples were incubated in the dark at 4 °C for 24 h before three technical replicates of 200 µL were transferred into a 96-well plate. Absorption of samples was immediately recorded at 630, 664, and 750 nm using a SpectraMax Paradigm microplate reader (Molecular Devices, US). Chlorophyll *a* content was calculated following Jeffrey & Humphrey (51):

$$\text{Chl } a \text{ [µg mL}^{-1}\text{]} = 11.43 \times (OD_{664} - OD_{750}) - 0.64 \times (OD_{630} - OD_{750})$$

Algal symbiont cell and chlorophyll *a* concentrations were corrected for sample volume and normalized to the surface area of the coral fragment.

Oxidative stress

Symbiotic reactive oxygen species (ROS) production was quantified from freshly isolated symbiont cells (52). For this, the tissue was removed from freshly sampled corals and homogenized as described above using sterile seawater. Washed symbiont cells were split into three technical replicates of 1 mL each in Eppendorf tubes and incubated for 30 min in the light (daily mean irradiance; 380 µmol photons m^{-2} s^{-1}) according to treatment temperature conditions. CellROX orange (Life Technologies, US) was added to the tubes at a final concentration of 5 µM, and cells were removed by centrifugation. 200 µL aliquots of the supernatant were immediately transferred into 96 well plates and incubated in the dark at 37 °C for 30 min. Relative ROS release (CellROX fluorescence) was quantified using a SpectraMax Paradigm microplate reader (Molecular Devices, US) at 468 nm excitation and 520 nm emission wavelength, respectively and normalized to the coral surface area.

Lipid peroxidation (quantified as total malondialdehyde content) was used as a proxy of oxidative stress in the host tissue. Coral tissue was removed from frozen coral fragments and homogenized as outlined above using ice-cold PBS buffer (1x). Symbiont cells were removed by centrifugation and three 100 µL aliquots of supernatant for each biological replicate were transferred into new Eppendorf tubes. The concentration of malondialdehyde in the samples was measured colorimetrically using the Lipid Peroxidation (MDA) Assay Kit (Abcam, US) according to the manufacturer's instructions. Malondialdehyde content was corrected for sample volume and normalized to the coral surface area.

Photosynthetic performance and respiration

Oxygen (O_2) production and consumption measurements were used to quantify net photosynthesis and respiration rates during light and dark incubations, respectively. For this purpose, individual coral fragments were transferred into 320 mL Nalgene incubation chambers filled with sterile seawater. Chambers were submerged in a water bath to maintain a constant temperature according to treatment conditions and stirred using magnetic stirrers. Specimens were left to acclimate for 30 min in the dark. Subsequently, O_2 concentrations were recorded every second for ~1 h at a constant light level of 380 µmol photons m^{-2} s^{-1} (daily mean irradiation) followed by ~1 h in the dark using FireSting O_2 optical oxygen meters (PyroScience, Germany).

Local linear regressions were performed using the 'LoLinR' R package v0.0.9 to objectively identify the best fitting linear regression to calculate O_2 fluxes during light and dark incubations, respectively (53). O_2 fluxes were corrected for seawater controls, normalized to the coral surface area, and converted into their carbon equivalents using photosynthetic and respiration quotients of 1.1. and 0.9, respectively (54). Gross photosynthesis rates were calculated as the sum of net photosynthesis (derived from light incubations) and respiration (derived from dark incubations) rates. The daily net photosynthetic carbon budget was calculated as the difference between daily fixation of carbon via gross photosynthesis (12 h) and the loss of fixed carbon via respiration (24 h).

Nutrient uptake/release

To assess net nutrient uptake and release rates, corals were incubated in 1 L incubation jars filled with 750 mL of artificial seawater for 24 hours. Artificial seawater composition was adapted from Harrison

et al. (55) to mimic Red Sea conditions (salinity = 39, pH = 8.1, 492.5 mM NaCl, 46.23 mM $MgCl_2$, 10.8 mM Na_2SO_4, 9.0 mM $CaCl_2$, 7.9 mM KCl, 2.5 mM $NaHCO_3$). Inorganic nutrients were added at elevated concentrations (5 µM NH_4^+, 5 µM NO_3^-, 2 µM PO_4^{3-}) compared to oligotrophic Red Sea water to allow for accurate measurements of nutrient depletion. Incubation water in jars was stirred using magnetic stirrers and maintained in a water bath mimicking aquaria conditions (light levels, temperature) according to treatment. Changes in nutrient concentrations during incubations were assessed by comparing start and end-point measurement. For analysis of inorganic nutrient concentrations, 50 mL of seawater were collected with a syringe, filtered (GFF, 0.22 µm), transferred into a Falcon tube, and immediately flash frozen for later analysis. For analysis of DOC concentrations, 10 mL of seawater was collected with a syringe, filtered (GFF, 0.22 µm), transferred into pre-combusted glass vials, acidified with concentrated phosphoric acid (pH < 2) and immediately sealed gas-tight for later analysis. Seawater samples were analyzed in triplicates using a SA3000/5000 nutrient auto-analyzer (SKALAR, Netherlands) and a TOC-L analyzer (Shimadzu, Japan) for inorganic and organic nutrient concentrations, respectively.

Isotope labeling & sample preparation

Corals were labeled with ^{13}C and ^{15}N to allow visualization and quantification of inorganic nutrient uptake and translocation in the coral–algae symbiosis using NanoSIMS imaging. Isotope labeling incubations were performed identically to nutrient uptake/release incubations explained above except that either HCO_3^- and NH_4^+ or NO_3^- were replaced with ^{13}C- or ^{15}N-enriched (~99.8 %) counterparts during artificial seawater preparation. After 24 h of incubation, small pieces (~5 mm) were clipped off the tip of coral fragments and immediately transferred into a fixative solution (1.25 % glutaraldehyde, 0.5 % paraformaldehyde in 0.1 M phosphate buffer). After 24 h of fixation at 4 °C, the samples were washed in PBS (1x) and decalcified using 0.1 M EDTA (4 °C, exchanged daily for 14 days). The samples were dissected into small pieces containing a row of individual polyps. The tissues were dehydrated in a series of increasing ethanol concentrations (50, 70, 90, 100 %) followed by 100% acetone. The tissues were then gradually infiltrated with SPURR resin of increasing concentrations (25, 50, 75, 100%). Subsequently, tissues were embedded in SPURR resin and cut into 170 nm sections using an Ultracut E microtome (Leica Microsystems, Germany) and mounted on silicon wafers for NanoSIMS imaging.

NanoSIMS imaging and analysis

Silicon wafers with attached sample sections were gold-coated and imaged with the NanoSIMS 50 ion probe (56) at the Center for Microscopy, Characterisation and Analysis at the University of Western Australia. Surfaces of samples were bombarded with a 16 keV primary Cs^+ beam focused to a spot size of about 100 nm with a current of ca. 2 pA. Secondary molecular ions $^{12}C^{12}C^-$, $^{12}C^{13}C^-$, $^{12}C^{14}N^-$, and $^{12}C^{15}N^-$ were simultaneously collected in electron multipliers at a mass resolution (M/ΔM) of about 8,000. Charge compensation was not necessary. At least fifteen images of different areas within the gastrodermis of the polyp tissue (30 µm raster with 256 × 256 pixels) were recorded for all targeted secondary molecular ions by rastering the primary beam across the sample with a dwell-time of 9 ms per pixel; six planes were recorded for each area. Image processing was performed using the ImageJ plugin OpenMIMS (National Resource for Imaging Mass Spectrometry, https://github.com/BWHCNI/OpenMIMS/wiki). After drift correction, the individual planes were summed and the $^{13}C/^{12}C$ or $^{15}N/^{14}N$ maps were expressed as a hue-saturation-intensity image (HSI),

where the color scale represents the isotope ratio. Assimilation of the isotope labels (atom % enrichment compared to unlabeled controls) was quantified for 25 (for $^{15}NH_4^+$-labeled samples) and 15 (for $^{15}NO_3^-$-labeled samples; 5 in the case of one colony) symbiont cells per coral fragment by circling individual Regions of Interest (ROIs) based on the $^{12}C^{14}N^-$ silhouette of the symbiont cells. To minimize the potential bias of varying symbiont densities (22), enrichment of the host tissue was measured only in the direct vicinity of each symbiont cell. For this, round ROIs were drawn with a radius of ca. 7 µm around the centroid of the symbiont cell and symbiont and symbiosome content was removed resulting in a doughnut-shaped ROI for the host tissue. To estimate the proportion of dividing or freshly divided symbiont cells, the mitotic index of the symbiont population was derived from $^{12}C^{14}N^-$ images. Specifically, the occurrence of symbiont cells in a dividing stage was counted in relation to the total occurrence of symbiont cells in the section of each coral colony (Fig. 3). Notably, the two-dimensional nature of NanoSIMS images may lead to an underestimation of the true Mitotic Index as not all dividing cells can be detected. However, this underestimation should be identical for all samples and thus not affect relative differences in the mitotic index between treatments.

RNA-Seq

Frozen coral fragments were placed into a Ziploc bag on ice and covered in 1.5 mL of ice-cold RLT tissue lysis buffer. Tissue was removed from the coral skeleton using air pressure for 1 min and the resulting tissue slurry in RLT buffer was immediately transferred into an Eppendorf tube and snap-frozen in liquid nitrogen. Total RNA was extracted from 500 µL defrosted coral slurry with the RNeasy Plant Mini Kit (Qiagen, Germany) according to the manufacturer's instructions. The concentration of total RNA was determined using Qubit BR RNA Assay Kit (Thermo Scientific, USA), and its integrity was evaluated using an Agilent 2100 Bioanalyzer and Nano Agilent RNA 6000 kit (Agilent Technologies, Santa Clara, CA, USA), according to the manufacturer's instructions. PolyA+ selection and subsequent mRNA library preparation were done using the TruSeq Stranded mRNA Library Prep kit (Illumina), according to the manufacturer's instruction. Resulting libraries (average fragments of 390 bp) were sequenced using the Illumina HiSeq4000 platform at the Bioscience Core lab facilities at KAUST to obtain paired-end reads of 150 bp.

Transcriptome analysis

Sequencing yielded an average of ~ 70 million reads per sample. Sequences were quality trimmed and Illumina adapters were removed using Trimmomatic v.0.39 (57). The successful removal of adapters was confirmed using FastQC v.0.11.5 (58). To remove symbiont sequence contamination, remaining sequences were split based on their best match to the gene models of *S. pistillata* (38) or *S. microadriaticum* (41) using BBsplit and sequences were mapped to the respective gene models using BBmap (BBtools v.37.10) (59). The expression of transcripts was quantified with Salmon v.1.0.0 (60) using the alignment-based mode. This produced an average of ~ 30 million and ~ 8 million mapped per sample for the coral host and algal symbiont, respectively. Effective transcript counts were used for identifying significantly differentially expressed genes ($p < 0.05$) between control and heat stress treatments using DeSeq2 v.1.26.0 (61). Differentially expressed genes were used to perform gene set enrichment analysis with topGO v.2.38.1 using the 'weight01' algorithm and no multiple test correction (62). Pathways of interest were further investigated by mapping differentially expressed genes to the Kyoto Encyclopedia of Genes and Genomes (KEGG) pathways using KEGG mapper v.3.2. (63). Genes were assigned to EuKaryotic Orthologous Groups (KOGs) categories using EggNOG 4.5.1

(64). Variance stabilizing transformation was applied to count data for principal component analysis and visualization based on total transcripts as well as subsets of individual KOG categories.

Coral surface area

All rates were normalized to coral fragment surface area calculated by 3D computer modeling (65). For this, ~40 photos were taken from coral fragments from different angles in front of a white background. The photos were uploaded to the Autodesk' Photo-to-3D cloud service (Autodesk, US) to generate 3D models of each fragment. The surface of 3D models was analyzed using ReCap Photo version 4.2.0.2 (Autodesk, US).

Statistical analysis

All statistical analyses were performed in R v.3.6.2 (66). Differences in physiological responses across treatments were analyzed in a paired design based on colony replicates. Normally distributed data (Shapiro-Wilk test $p < 0.05$) were tested with a paired two-sided t-test. Otherwise, data were analyzed using a Wilcoxon signed-rank test. NanoSIMS measurements of relative ^{13}C and ^{15}N abundance in the host and symbiont tissue/cells were analyzed using linear mixed models with treatment as a fixed and colony as a random effect using the "lme4" R package v.1.1-21 (67). NanoSIMS data were log-transformed prior to analysis to account for skewing of data. Differences in expression profiles were analyzed with permutational multivariate analysis of variance (PERMANOVA) with treatment and colony as explanatory variables as implemented in the "vegan" R package v.2.5-6 (68).

Acknowledgments

We would like to thank Dr. Zenon B. Batang and Dr. Nabeel M. Alikunhi for their continuous support and assistance with aquaria maintenance. Further, Ioannis Georgakakis, Mustafa Altunkaya, Gabriela Perna, Prof. Dr. Matt Kilburn are acknowledged for their help and support with sample processing and data analysis. NR, CP, AC, MP, JBR & CRV are supported by the KAUST competitive research grant URF/1/3400-01-01. CRV also acknowledges baseline funding from KAUST.

Data availability

Detailed results of gene expression analyses are provided as Supplementary Data files. All raw data associated with this manuscript will be made publicly available via the Dryad data repository upon acceptance. Additionally, raw sequencing data will be deposited in the NCBI Sequence Read Archive under BioProject accession number PRJNA638625 upon acceptance of the manuscript.

References

1. N. Knowlton, J. B. C. Jackson, Shifting baselines, local impacts, and global change on coral reefs. *PLoS Biol.* **6**, e54 (2008).

2. O. Hoegh-Guldberg, *et al.*, Coral reefs under rapid climate change and ocean acidification. *Science* **318**, 1737–1742 (2007).

3. T. P. Hughes, *et al.*, Global warming and recurrent mass bleaching of corals. *Nature* **543**, 373–377 (2017).

4. T. P. Hughes, *et al.*, Coral reefs in the Anthropocene. *Nature* **546**, 82–90 (2017).

5. F. Rohwer, V. Seguritan, F. Azam, Diversity and distribution of coral-associated bacteria. *Mar. Ecol. Prog. Ser.* **243**, 1-10 (2002).

6. J. Bellworthy, M. Fine, Beyond peak summer temperatures, branching corals in the Gulf of Aqaba are resilient to thermal stress but sensitive to high light. *Coral Reefs* **36**, 1071–1082 (2017).

7. C. Pogoreutz, *et al.*, Sugar enrichment provides evidence for a role of nitrogen fixation in coral bleaching. *Glob. Chang. Biol.* **23**, 3838–3848 (2017).

8. D. J. Suggett, D. J. Smith, Coral bleaching patterns are the outcome of complex biological and environmental networking. *Glob. Chang. Biol.* **26**, 68–79 (2020).

9. E. Rosenberg, A. Kushmaro, E. Kramarsky-Winter, E. Banin, L. Yossi, The role of microorganisms in coral bleaching. *ISME J.* **3**, 139–146 (2009).

10. A. H. Baird, R. Bhagooli, P. J. Ralph, S. Takahashi, Coral bleaching: the role of the host. *Trends Ecol. Evol.* **24**, 16–20 (2009).

11. M. J. H. van Oppen, J. K. Oliver, H. M. Putnam, R. D. Gates, Building coral reef resilience through assisted evolution. *Proc. Natl. Acad. Sci. U.S.A.* **112**, 2307–2313 (2015).

12. V. M. Weis, Cellular mechanisms of Cnidarian bleaching: stress causes the collapse of symbiosis. *J. Exp. Biol.* **211**, 3059–3066 (2008).

13. D. J. Smith, D. J. Suggett, N. R. Baker, Is photoinhibition of zooxanthellae photosynthesis the primary cause of thermal bleaching in corals? *Glob. Chang. Biol.* **11**, 1–11 (2005).

14. M. P. Lesser, Oxidative stress causes coral bleaching during exposure to elevated temperatures. *Coral Reefs* **16**, 187–192 (1997).

15. M. P. Lesser, Elevated temperatures and ultraviolet radiation cause oxidative stress and inhibit photosynthesis in symbiotic dinoflagellates. *Limnol. Oceanogr.* **41**, 271–283 (1996).

16. D. Tolleter, *et al.*, Coral bleaching independent of photosynthetic activity. *Curr. Biol.* **23**, 1782–1786 (2013).

17. T. Krueger, *et al.*, Differential coral bleaching - contrasting the activity and response of enzymatic antioxidants in symbiotic partners under thermal stress. *Comp. Biochem. Physiol. A Mol. Integr. Physiol.* **190**, 15–25 (2015).

18. J. M. Diaz, *et al.*, Species-specific control of external superoxide levels by the coral holobiont during a natural bleaching event. *Nat. Commun.* **7**, 13801 (2016).

19. L. Muscatine, J. W. Porter, Reef corals: mutualistic symbioses adapted to nutrient-poor environments. *Bioscience* **27**, 454–460 (1977).

20. P. G. Falkowski, Z. Dubinsky, L. Muscatine, J. W. Porter, Light and the bioenergetics of a symbiotic coral. *Bioscience* **34**, 705–709 (1984).

21. M. P. Lesser, Using energetic budgets to assess the effects of environmental stress on corals: are we measuring the right things? *Coral Reefs* **32**, 25–33 (2013).

22. T. Krueger, *et al.*, Intracellular competition for nitrogen controls dinoflagellate population density in corals. *Proc. Roy. Soc. B* **287**, 20200049 (2020).

23. G. Cui, *et al.*, Host-dependent nitrogen recycling as a mechanism of symbiont control in Aiptasia. *PLoS Genet.* **15**, e1008189 (2019).

24. L. Ezzat, J.-F. Maguer, R. Grover, C. Ferrier-Pagès, New insights into carbon acquisition and exchanges within the coral–dinoflagellate symbiosis under NH_4^+ and NO_3^- supply. *Proc. Roy. Soc. B* **282**, 20150610 (2015).

25. N. Rädecker, C. Pogoreutz, C. R. Voolstra, J. Wiedenmann, C. Wild, Nitrogen cycling in corals: the key to understanding holobiont functioning? *Trends Microbiol.* **23**, 490–497 (2015).

26. L. A. Morris, C. R. Voolstra, K. M. Quigley, D. G. Bourne, L. K. Bay, Nutrient availability and metabolism affect the stability of coral–Symbiodiniaceae symbioses. *Trends Microbiol.* **27**, 678–689 (2019).

27. I. E. Conti-Jerpe, *et al.*, Trophic strategy and bleaching resistance in reef-building corals. *Sci. Adv.* **6**, eaaz5443 (2020).

28. E. Beraud, F. Gevaert, C. Rottier, C. Ferrier-Pages, The response of the scleractinian coral *Turbinaria reniformis* to thermal stress depends on the nitrogen status of the coral holobiont. *J. Exp. Biol.* **216**, 2665–2674 (2013).

29. J. Wiedenmann, *et al.*, Nutrient enrichment can increase the susceptibility of reef corals to bleaching. *Nat. Clim. Chang.* **3**, 160–164 (2012).

30. L. Ezzat, J.-F. Maguer, R. Grover, C. Ferrier-Pagès, Limited phosphorus availability is the Achilles heel of tropical reef corals in a warming ocean. *Sci. Rep.* **6**, 31768 (2016).

31. D. M. Baker, C. J. Freeman, J. C. Y. Wong, M. L. Fogel, N. Knowlton, Climate change promotes parasitism in a coral symbiosis. *ISME J.* **12**, 921–930 (2018).

32. E. M. Gibbin, *et al.*, Short-term thermal acclimation modifies the metabolic condition of the coral holobiont. *Front. Mar. Sci.* **5** (2018).

33. M. Fine, H. Gildor, A. Genin, A coral reef refuge in the Red Sea. *Glob. Chang. Biol.* **19**, 3640–3647 (2013).

34. E. O. Osman, *et al.*, Thermal refugia against coral bleaching throughout the northern Red Sea. *Glob. Chang. Biol.* **24**, e474–e484 (2018).

35. T. Krueger, *et al.*, Common reef-building coral in the Northern Red Sea resistant to elevated temperature and acidification. *Roy. Soc. Open Sci.* **4**, 170038 (2017).

36. R. Berkelmans, Time-integrated thermal bleaching thresholds of reefs and their variation on the

Great Barrier Reef. *Mar. Ecol. Prog. Ser.* **229**, 73–82 (2002).

37. J. H. Brown, J. F. Gillooly, A. P. Allen, V. M. Savage, G. B. West, Toward a metabolic theory of ecology. *Ecology* **85**, 1771–1789 (2004).

38. C. R. Voolstra, *et al.*, Comparative analysis of the genomes of *Stylophora pistillata* and *Acropora digitifera* provides evidence for extensive differences between species of corals. *Sci. Rep.* **7**, 17583 (2017).

39. O. Rahav, Z. Dubinsky, Y. Achituv, P. G. Falkowski, D. C. Smith, Ammonium metabolism in the zooxanthellate coral, *Stylophora pistillata*. *Proc. Roy. Soc. B* **236**, 325–337 (1989).

40. N. Dudler, D. J. Miller, Characterization of two glutamate dehydrogenases from the symbiotic microalga *Symbiodinium microadriaticum* isolated from the coral *Acropora formosa*. *Mar. Biol.* **97**, 427–430 (1988).

41. M. Aranda, *et al.*, Genomes of coral dinoflagellate symbionts highlight evolutionary adaptations conducive to a symbiotic lifestyle. *Sci. Rep.* **6**, 39734 (2016).

42. E. Ocaña-Pallarès, S. R. Najle, C. Scazzocchio, I. Ruiz-Trillo, Reticulate evolution in eukaryotes: origin and evolution of the nitrate assimilation pathway. *PLoS Genet.* **15**, e1007986 (2019).

43. N. Rädecker, C. Pogoreutz, C. Wild, C. R. Voolstra, Stimulated respiration and net photosynthesis in *Cassiopeia* sp. during glucose enrichment suggests in hospite CO_2 limitation of algal endosymbionts. *Front. Mar. Sci.* **4**, 16 (2017).

44. R. Cunning, A. C. Baker, Excess algal symbionts increase the susceptibility of reef corals to bleaching. *Nat. Clim. Chang.* **3**, 259–262 (2012).

45. N. Rädecker, *et al.*, Using Aiptasia as a model to study metabolic interactions in Cnidarian-*Symbiodinium* symbioses. *Front. Physiol.* **9**, 214 (2018).

46. K. R. N. Anthony, S. R. Connolly, O. Hoegh-Guldberg, Bleaching, energetics, and coral mortality risk: effects of temperature, light, and sediment regime. *Limnol. Oceanogr.* **52**, 716–726 (2007).

47. R. W. Buddemeier, D. G. Fautin, Coral bleaching as an adaptive mechanism. *BioScience* **43**, 320–326 (1993).

48. C. A. Downs, *et al.*, Oxidative stress and seasonal coral bleaching. *Free Radic. Biol. Med.* **33**, 533–543 (2002).

49. H. Malcolm, H. April, The magnesium inhibition and arrested phagosome hypotheses: new perspectives on the evolution and ecology of *Symbiodinium* symbioses. *Biol. Rev. Camb. Philos. Soc.* **87**, 804–821 (2012).

50. T. Bieri, M. Onishi, T. Xiang, A. R. Grossman, J. R. Pringle, Relative contributions of various cellular mechanisms to loss of algae during Cnidarian bleaching. *PLoS One* **11**, e0152693 (2016).

51. S. W. Jeffrey, G. F. Humphrey, New spectrophotometric equations for determining chlorophylls a, b, c1 and c2 in higher plants, algae and natural phytoplankton. *Biochem. Physiol. Pflanzen* **167**, 191–194 (1975).

52. M. J. Cziesielski, *et al.*, Multi-omics analysis of thermal stress response in a zooxanthellate cnidarian reveals the importance of associating with thermotolerant symbionts. *Proc. Roy. Soc. B*

285, 20172654 (2018).

53. C. Olito, C. R. White, D. J. Marshall, D. R. Barneche, Estimating monotonic rates from biological data using local linear regression. *J. Exp. Biol.* **220**, 759–764 (2017).

54. L. Muscatine, L. R. McCloskey, R. E. Marian, Estimating the daily contribution of carbon from zooxanthellae to coral animal respiration. *Limnol. Oceanogr.* **26**, 601–611 (1981).

55. P. J. Harrison, R. E. Waters, F. J. R. Taylor, A broad spectrum artificial sea water medium for coastal and open ocean phytoplankton. *J. Phycol.* **16**, 28–35 (1980).

56. P. Hoppe, S. Cohen, A. Meibom, NanoSIMS: technical aspects and applications in cosmochemistry and biological biochemistry. *Geostand. Geoanal. Res.* **37**, 111–154 (2013).

57. A. M. Bolger, M. Lohse, B. Usadel, Trimmomatic: a flexible trimmer for Illumina sequence data. *Bioinformatics* **30**, 2114–2120 (2014).

58. S. Andrews, et al., FastQC: a quality control tool for high throughput sequence data. *URL http://www.bioinformatics.babraham.ac.uk/projects/fastqc* (2010).

59. B. Bushnell, BBTools software package. *URL http://sourceforge. net/projects/bbmap* (2014).

60. R. Patro, G. Duggal, M. I. Love, R. A. Irizarry, C. Kingsford, Salmon provides fast and bias-aware quantification of transcript expression. *Nat. Methods* **14**, 417–419 (2017).

61. M. I. Love, W. Huber, S. Anders, Moderated estimation of fold change and dispersion for RNA-seq data with DESeq2. *Genome Biol.* **15**, 550 (2014).

62. A. Alexa, J. Rahnenfuhrer, topGO: enrichment analysis for gene ontology. *R package version* **2**, 2010 (2010).

63. M. Kanehisa, Y. Sato, KEGG Mapper for inferring cellular functions from protein sequences. *Protein Sci.* **29**, 28–35 (2020).

64. J. Huerta-Cepas, *et al.*, eggNOG 4.5: a hierarchical orthology framework with improved functional annotations for eukaryotic, prokaryotic and viral sequences. *Nucleic Acids Res.* **44**, D286–93 (2016).

65. A. Lavy, *et al.*, A quick, easy and non-intrusive method for underwater volume and surface area evaluation of benthic organisms by 3D computer modelling. *Methods Ecol. Evol.* **6**, 521–531 (2015).

66. R. Core Team, Others, R: a language and environment for statistical computing. *R Foundation for statistical computing, Vienna* (2020).

67. D. Bates, Fitting linear mixed models in R. *R news* **5**, 27–30 (2005).

68. J. Oksanen, *et al.*, The vegan package. *Community ecology package* **10**, 631–637 (2007).

Figures and Tables

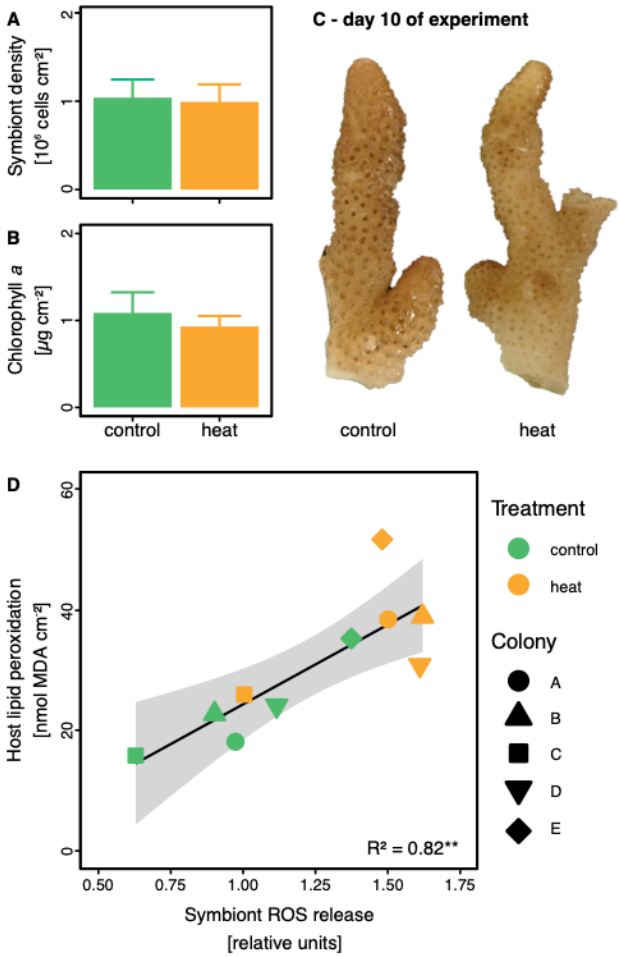

Figure 1. State of symbiosis on day 10 of heat stress. (A,B,C) Corals showed no significant differences in symbiont densities or chlorophyll *a* content and no visual signs of bleaching. (D) Relative release of ROS from freshly isolated symbionts increased during heat stress and correlated with levels of oxidative stress (measured as lipid peroxidation) in the host tissue. Bars indicate the mean ± SE. The line displays best-fitting linear regression. The shaded area indicates the 95 % confidence interval. The R^2 value indicates the amount of variation explained by the linear regression.

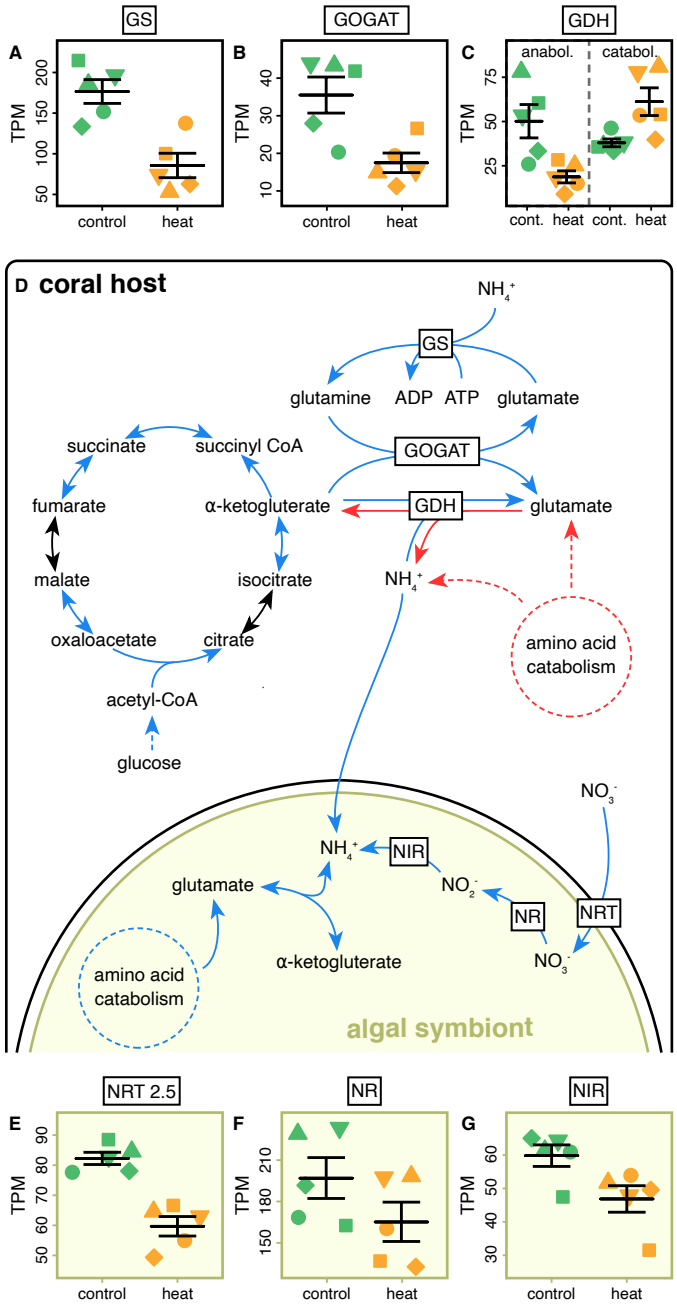

Figure 2. Regulation of coral host and algal symbiont gene expression on day 10 of heat stress. (A-C) Mean gene expression of significantly differentially expressed key genes in the amino acid metabolism of the coral host. (D) Overview of how highlighted metabolic pathways of host and algal symbiont may interact to alter nutrient cycling in the symbiosis. (F-G) Mean gene expression of significant differentially expressed key genes in the nitrate (NO_3^-) assimilation of algal symbionts. Blue arrows indicate a significant downregulation whereas red arrows indicate a significant upregulation of gene expression during heat stress. Lines and error bars indicate mean ± SE. GDH = glutamate dehydrogenase, GOGAT = glutamate synthase, GS = glutamine synthetase, NIR = nitrite reductase, NR = nitrate reductase, NRT = nitrate transporter, TPM = transcripts per million. For a complete list of differentially expressed genes as well as significant GO terms see Suppl. Data.

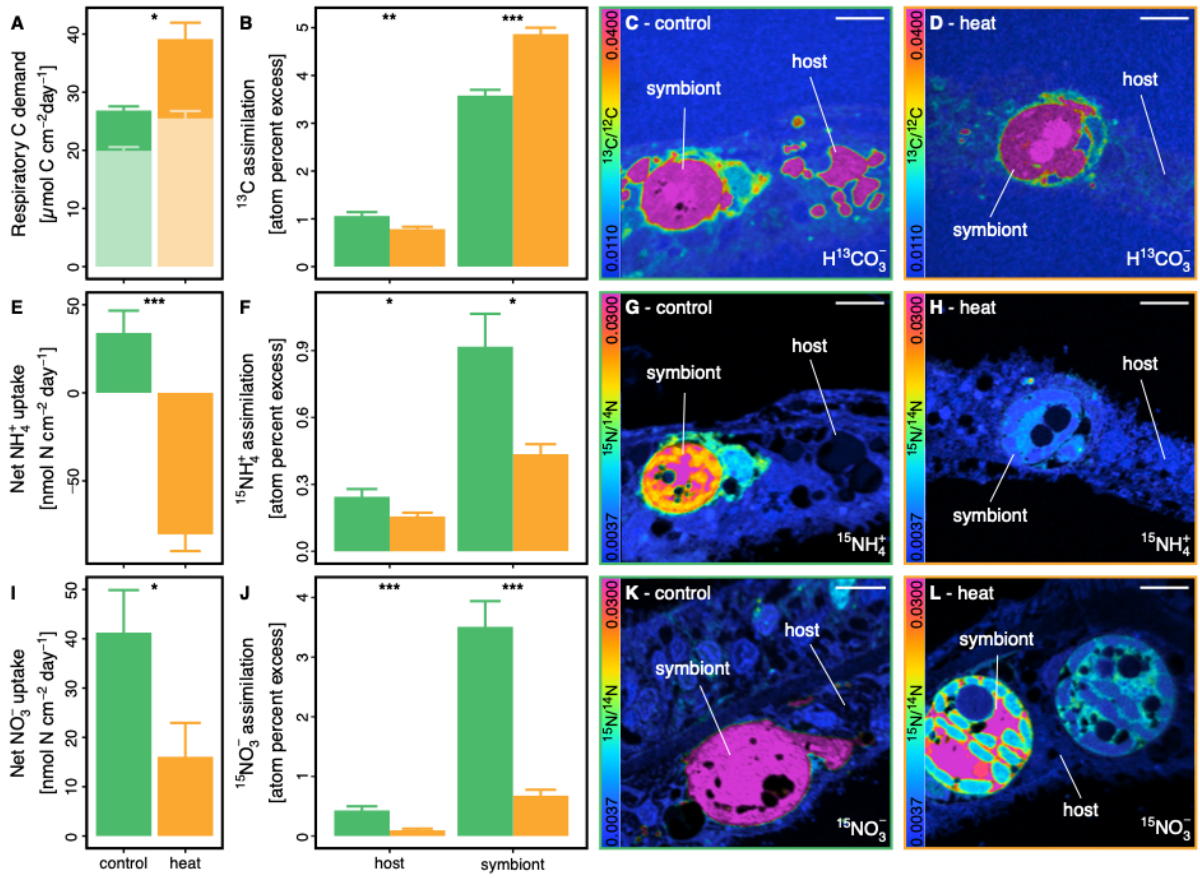

Figure 3. Symbiotic assimilation and fate of carbon and nitrogen on day 10 of heat stress. (A) Respiratory carbon consumption of the holobiont derived from oxygen fluxes. Pale bars indicate carbon demand fulfilled by gross photosynthetic production. (B) Assimilation of ^{13}C-bicarbonate ($H^{13}CO_3^-$) into host and symbiont cells, respectively, based on NanoSIMS imaging (C,D). (E) Net ammonium (NH_4^+) uptake of coral fragments from seawater. Negative values indicated a net release of NH_4^+ from the holobiont. (G) Assimilation of $^{15}NH_4^+$ into host and symbiont cells respectively derived from NanoSIMS imaging (G,H). (I) Net nitrate (NO_3^-) uptake of coral fragments from seawater. (J) Assimilation of $^{15}NO_3^-$ into host and symbiont cells respectively derived from NanoSIMS imaging (K,L). Bars indicate mean ± SE. Asterisks indicated significant differences between treatments. White scale bars in the top right of NanoSIMS images indicate 5 µm.

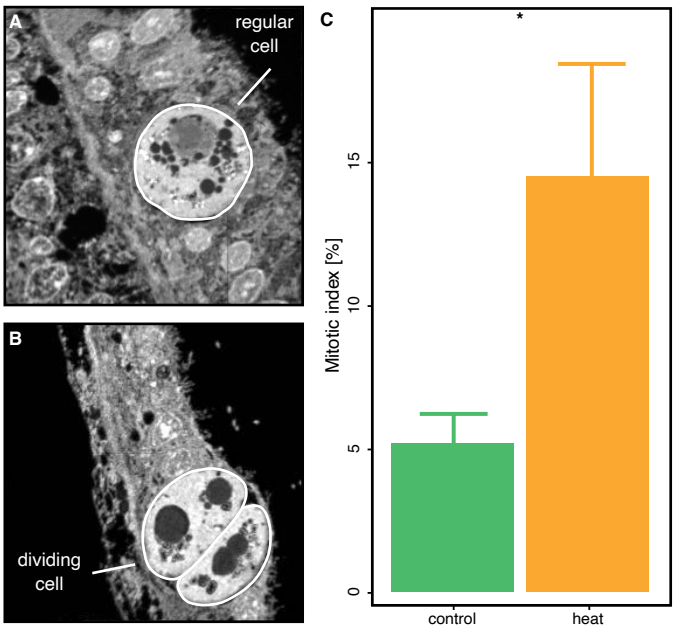

Figure 4. Proportion of dividing algal symbiont cells on day 10 of heat stress. NanoSIMS images for $^{12}C^{14}N^-$ were used to quantify the abundance of (A) regular and (B) dividing algal symbiont cells in the coral tissue sections. (C) These data were used to calculate the proportion of dividing cells in the algal symbiont population. Note that this mitotic index reflects an underestimation of the true proportion of dividing cells due to the two-dimensional nature of NanoSIMS images. Bars indicate mean ± SE. Asterisks indicated significant differences between treatments.

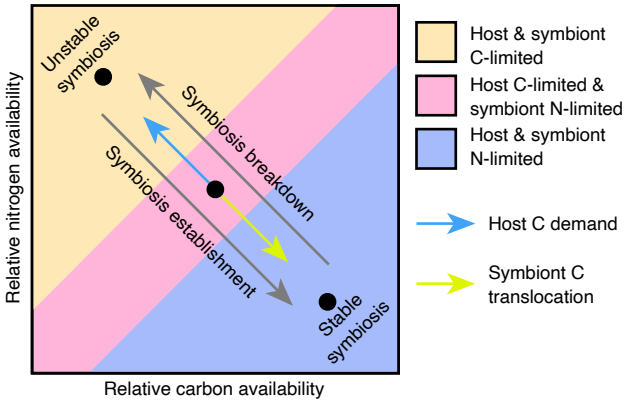

Figure 5. Model outlining the dynamic transition between a stable and unstable state of the coral–algal symbiosis based on the nutritional state of host and symbiont. In this model, the state of the symbiosis depends on the dynamic balance of metabolic carbon (C) demand of the host and C translocation by algal symbionts. In a stable state, C translocation by algal symbionts fulfils or exceeds the metabolic C demands of the host, thereby arresting the symbiosis in a nitrogen (N)-limited state. Environmental stressors, such as rapid warming, may cause a proportional increase of host C requirements over symbiont C translocation resulting in a positive feedback loop that destabilizes carbon cycling in the symbiosis and eventually shifts the symbiosis towards a C-limited stage. Likewise, the rapid proliferation of algal symbionts during the (re-)establishment of the symbiosis will accordingly increase competition for available N between symbionts. Thereby, the symbiosis is gradually shifting towards a nitrogen-limited state in which C translocation and recycling are maximized.

Supplementary Information

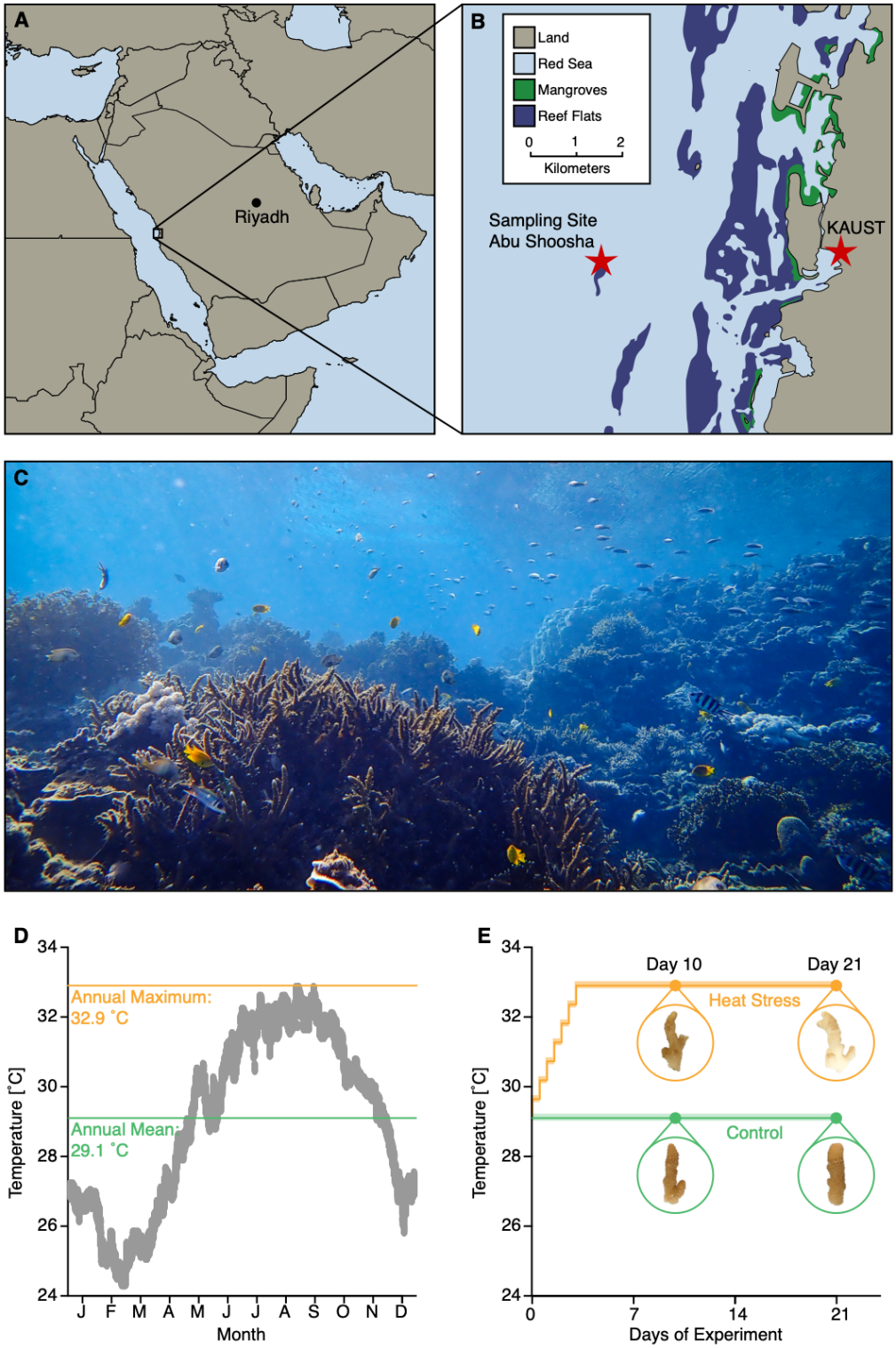

Figure S1. Overview of the sampling site and its environmental conditions. (A,B) Coral colonies were collected at Abu Shoosha reef (22°18'16.3''N; 39°02'57.7''E) approximately 5 km off the central Red Sea coast of Saudi Arabia. (C) Abu Shoosha is a shallow-water reef with pronounced seasonality. (D) The temperature profile for Abu Shoosha at 5m water depth for the year 2017 was used to identify the annual mean and maximum temperature of a representative year without mass-bleaching. (E) Based on this information, corals were exposed to either annual mean temperatures (29.1 ˚C, control) or annual maximum temperatures (32.9 ˚C, heat stress) for a 21-day aquaria experiment. Corals were sampled on days 10 and 21 of the experiment.

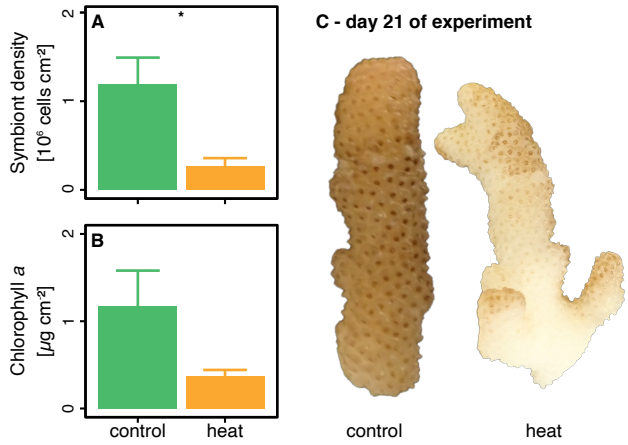

Figure S2. State of symbiosis on day 21 of the experiment. (A,B,C) Corals showed clear visual signs of bleaching and a significant decline in symbiont densities as well as a reduction in chlorophyll *a* content. Bars indicate mean ± SE. Asterisks indicated significant differences between treatments.

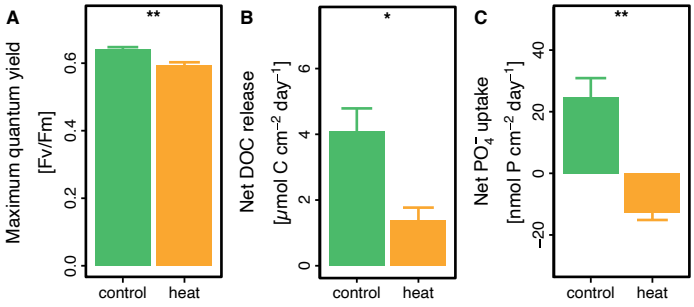

Figure S3. Photophysiology and nutrient fluxes on day 10 of the experiment. (A) Maximum photosynthetic quantum yield of fragments after 30 min dark acclimation. (B) Net dissolved organic carbon (DOC) release from the coral holobiont. (C) Net phosphate (PO_4^-) uptake from the coral holobiont. Negative bars indicate a net release of PO_4^-. Bars indicate mean ± SE. Asterisks indicated significant differences between treatments.

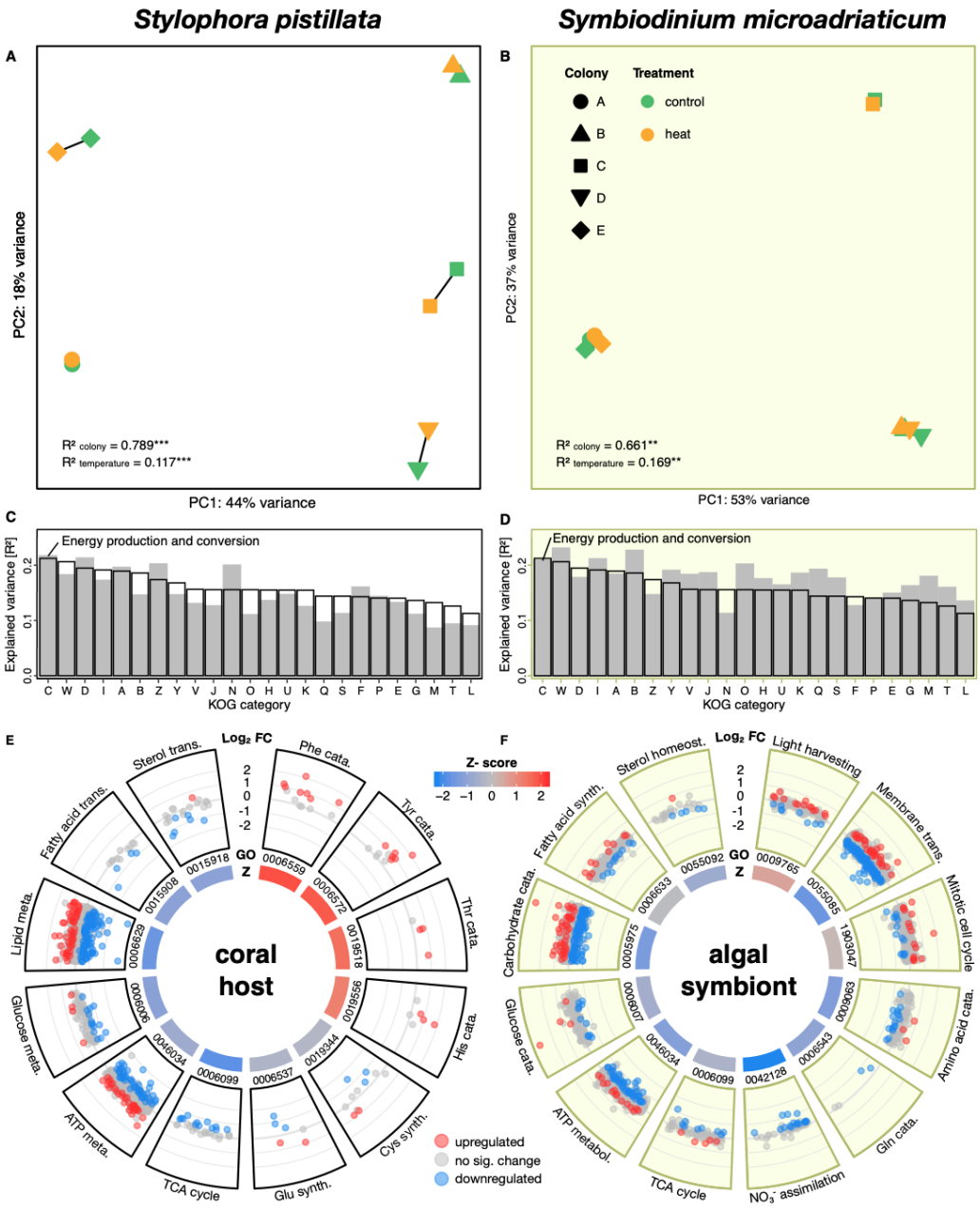

Figure S4. Gene expression of (A,C,E) *Stylophora pistillata* and (B,D,F) *Symbiodinium microadriaticum* on day 10 of heat stress. (A,B) Principal component analysis of gene expression profiles. Lines connect control (green) and heat stress (orange) samples from the same colony of origin. (C,D) Permutational analysis of variance (Permanova) analyses of the proportion of variance in gene expression explained by the temperature treatment for each subset of genes related to individual EuKaryotic Orthologous Groups (KOGs). Grey bars indicate results for the respective symbiotic partner whereas empty black bars indicate mean responses of both symbiotic partners combined. (E,F) Selected significantly enriched Gene Ontology (GO) terms related to carbon and amino acid metabolism as well as inorganic nutrient transport. Points indicate mean $\log_2$ fold change of expression of genes associated to GO terms in heat stress compared to control conditions. Blue points indicate significant downregulation, whereas red points indicate significant upregulation. Boxes below individual GO terms indicate the overall direction of regulation (Z-score). ATP = adenosine triphosphate, cata. = catabolism, Cys = cysteine, Gln = glutamine, Glu = glutamate, His = histidine, homeost. = homeostasis, meta. = metabolism, Ser = serine, Phe = phenylalanine, synth. = biosynthesis, TCA = tricarboxylic acid, trans. = transport, Tyr = tyrosine. See Table S2, S3 for an overview of Permanova results. For a complete list of differentially expressed genes as well as significant GO terms see Suppl. Data.

Table S1. Results of statistical analysis for physiological and NanoSIMS measurements. Physiological measurements were analyzed in a paired design based on the mother colony. Likewise, log-transformed NanoSIMS data were analyzed in linear mixed models using colony of origin as a random effect.

Day	Response parameter	Test	Replicates	Statistic	*p*
21	Symbiont density	Paired *t*-test	10	3.728	0.020
21	Chlorophyll *a* content	Paired Wilcoxon	10	15.000	0.063
10	Symbiont density	Paired *t*-test	10	0.347	0.746
10	Chlorophyll *a* content	Paired *t*-test	10	0.454	0.674
10	Photosynthetic efficiency	Paired *t*-test	10	6.778	0.002
10	Gross photosynthesis	Paired *t*-test	10	-3.469	0.026
10	Respiration	Paired *t*-test	10	-3.762	0.020
10	Dissolved organic carbon release	Paired *t*-test	10	3.841	0.018
10	NH_4^+ uptake	Paired *t*-test	10	-15.991	0.001
10	NO_3^- uptake	Paired *t*-test	10	-3.041	0.038
10	PO_4^{3-} uptake	Paired *t*-test	10	-6.328	0.003
10	ROS release (symbiont)	Paired *t*-test	10	-4.407	0.012
10	Lipid peroxidation (host)	Paired *t*-test	10	-5.735	0.005
10	Mitotic index	Paired *t*-test	10	-2.896	0.044
10	$H^{13}CO_3^-$ assimilation (host)	Linear mixed model	250	8.000	0.005
10	$H^{13}CO_3^-$ assimilation (symbiont)	Linear mixed model	250	52.88	0.001
10	$^{15}NH_4^+$ assimilation (host)	Linear mixed model	250	6.330	0.013
10	$^{15}NH_4^+$ assimilation (symbiont)	Linear mixed model	250	5.528	0.020
10	$^{15}NO_3^-$ assimilation (host)	Linear mixed model	140	40.715	0.001
10	$^{15}NO_3^-$ assimilation (host)	Linear mixed model	140	72.343	0.001

Table S2. Permutational multivariate analysis of variance (PERMANOVA) on the effects of mother colony and temperature on the transcriptomic response of *Stylophora pistillata.* Responses were assessed for the global transcriptome as well as for specific subsets of genes assigned to individual EuKaryotic Orthologous Groups (KOGs) categories.

		Colony effect			Temperature effect		
Response category	**Genes**	**R^2**	**F**	***p***	**R^2**	**F**	***p***
Global transcriptome	25769	0.789	8.362	0.001	0.117	4.938	0.001
KOG categories							
D - Cell cycle control, cell division, chromosome partitioning	406	0.692	7.218	0.001	0.212	8.867	0.001
M - Cell wall/membrane/envelope biogenesis	343	0.838	10.959	0.001	0.086	4.474	0.001
N - Cell motility	30	0.656	4.539	0.002	0.200	5.521	0.001
O - Post-translational modification, protein turnover, and chaperones	2125	0.788	7.690	0.001	0.110	4.296	0.001
T - Signal transduction mechanisms	3288	0.810	8.349	0.001	0.093	3.840	0.001
U - Intracellular trafficking, secretion, and vesicular transport	852	0.715	5.167	0.001	0.146	4.231	0.001
V - Defense mechanisms	128	0.736	5.473	0.001	0.130	3.871	0.002
W - Extracellular structures	120	0.666	4.393	0.001	0.182	4.801	0.001
Y - Nuclear structure	40	0.760	8.091	0.001	0.146	6.214	0.001
Z - Cytoskeleton	416	0.655	4.559	0.001	0.202	5.615	0.001
A - RNA processing and modification	500	0.712	7.694	0.001	0.196	8.455	0.001
B - Chromatin structure and dynamics	309	0.812	19.354	0.001	0.146	13.869	0.001
J - Translation, ribosomal structure and biogenesis	566	0.735	5.296	0.001	0.126	3.629	0.003
K - Transcription	1135	0.782	8.342	0.001	0.125	5.326	0.001
L - Replication, recombination and repair	1152	0.858	16.484	0.001	0.090	6.938	0.001
C - Energy production and conversion	365	0.636	4.306	0.001	0.217	5.865	0.001
E - Amino acid transport and metabolism	1072	0.767	7.561	0.001	0.132	5.200	0.001
F - Nucleotide transport and metabolism	184	0.744	7.753	0.001	0.160	6.662	0.001
G - Carbohydrate transport and metabolism	898	0.777	6.885	0.001	0.111	3.918	0.001
H - Coenzyme transport and metabolism	146	0.691	3.971	0.001	0.135	3.115	0.007
I - Lipid transport and metabolism	432	0.719	6.573	0.001	0.172	6.293	0.001
P - Inorganic ion transport and metabolism	595	0.720	5.269	0.001	0.143	4.179	0.001
Q - Secondary metabolites biosynthesis, transport, and catabolism	395	0.792	7.118	0.002	0.096	3.465	0.024
R - General function prediction only	0	NA	NA	NA	NA	NA	NA
S - Function unknown	4820	0.806	9.839	0.001	0.112	5.465	0.001

Table S3. Permutational multivariate analysis of variance (PERMANOVA) on the effects of mother colony and temperature on the transcriptomic response of *Symbiodinium microadriaticum*. Responses were assessed for the global transcriptome as well as for specific subsets of genes assigned to individual EuKaryotic Orthologous Groups (KOGs) categories.

		Colony effect			Temperature effect		
Response category	**Genes**	**R^2**	**F**	***p***	**R^2**	**F**	***p***
Global transcriptome	49109	0.661	3.877	0.002	0.169	3.959	0.002
KOG categories							
D - Cell cycle control, cell division, chromosome partitioning	269	0.646	3.641	0.001	0.177	3.994	0.001
M - Cell wall/membrane/envelope biogenesis	298	0.693	5.412	0.001	0.179	5.599	0.001
N - Cell motility	30	0.770	6.516	0.002	0.112	3.795	0.038
O - Post-translational modification, protein turnover, and chaperones	1240	0.640	4.049	0.001	0.201	5.096	0.001
T - Signal transduction mechanisms	1149	0.694	4.747	0.001	0.159	4.353	0.001
U - Intracellular trafficking, secretion, and vesicular transport	609	0.690	4.729	0.001	0.164	4.483	0.002
V - Defense mechanisms	157	0.693	5.553	0.001	0.183	5.861	0.002
W - Extracellular structures	29	0.586	3.197	0.001	0.230	5.025	0.001
Y - Nuclear structure	20	0.468	1.366	0.171	0.190	2.221	0.046
Z - Cytoskeleton	417	0.713	5.071	0.001	0.146	4.156	0.005
A - RNA processing and modification	404	0.624	3.242	0.001	0.183	3.807	0.001
B - Chromatin structure and dynamics	124	0.564	2.685	0.001	0.226	4.314	0.001
J - Translation, ribosomal structure and biogenesis	685	0.627	3.353	0.001	0.186	3.971	0.001
K - Transcription	332	0.655	4.100	0.001	0.185	4.623	0.001
L - Replication, recombination and repair	1497	0.693	4.023	0.001	0.135	3.141	0.006
C - Energy production and conversion	484	0.648	4.497	0.001	0.208	5.782	0.001
E - Amino acid transport and metabolism	620	0.712	5.118	0.001	0.149	4.274	0.004
F - Nucleotide transport and metabolism	204	0.763	6.860	0.001	0.126	4.537	0.002
G - Carbohydrate transport and metabolism	998	0.702	5.160	0.001	0.162	4.766	0.001
H - Coenzyme transport and metabolism	307	0.644	3.549	0.001	0.175	3.857	0.001
I - Lipid transport and metabolism	438	0.624	3.791	0.001	0.211	5.123	0.001
P - Inorganic ion transport and metabolism	641	0.770	8.358	0.001	0.138	6.008	0.001
Q - Secondary metabolites biosynthesis, transport, and catabolism	490	0.656	4.311	0.001	0.192	5.048	0.001
R - General function prediction only	0	NA	NA	NA	NA	NA	NA
S - Function unknown	2571	0.652	3.808	0.001	0.176	4.114	0.001